

# Measuring the Balmer jump and the effective gravity in FGK stars

Michael S. Bessell

*RSAA, The Australian National University, Mt Stromlo, Cotter Rd, Weston, ACT 2611, Australia*

## ABSTRACT

It is difficult to accurately measure the effective gravity ( $\log g$ ) in late-type stars using broadband (eg. UBV or SDSS) or intermediate-band (uvby) photometric systems, especially when the stars can cover a range of metallicities and reddenings. However, simple spectroscopic observational and data reduction techniques can yield accurate values for  $\log g$  through comparison of the Balmer jumps of low-resolution spectra with recent grids of synthetic flux spectra.

*Subject headings:* techniques: spectroscopic — stars: atmospheres — stars: fundamental parameters (temperatures, gravities) — stars: late-type — stars: Population II

## 1. Introduction

The abundance analyses of the oldest stars in the galaxy are of great importance to understand which elements were created during the life and death of the first generation of stars and how the fraction of heavy elements built up through the evolution of subsequent generations of stars. The effective temperature is the most important stellar atmosphere parameter to assign in the determination of abundances, but for those elements only represented by lines of the neutral species, it is necessary to establish the electron pressure or the effective gravity of the star. This is because hotter than about 4500K most of the heavy elements are once ionised and significant corrections are required to determine the total element abundances from the neutral species. Theoretical isochrones for a range of metallicities and ages are readily available (Pietrinferni et al. 2006; VandenBerg 2000; Salasnich et al. 2000) and the normal  $\log (L/L_{\odot})$  versus  $\log T_e$  relations can be readily transformed to  $\log g$  versus  $T_e$  ( $\log g = 4 \log T_e - \log (L/L_{\odot}) - 10.608$ ).

Fig. 1 shows a typical halo isochrone for age 12 Gyr. For old stars (age  $> 10$  Gyr), the shape of the isochrone changes little as the main-sequence turn-off (TO) moves to cooler

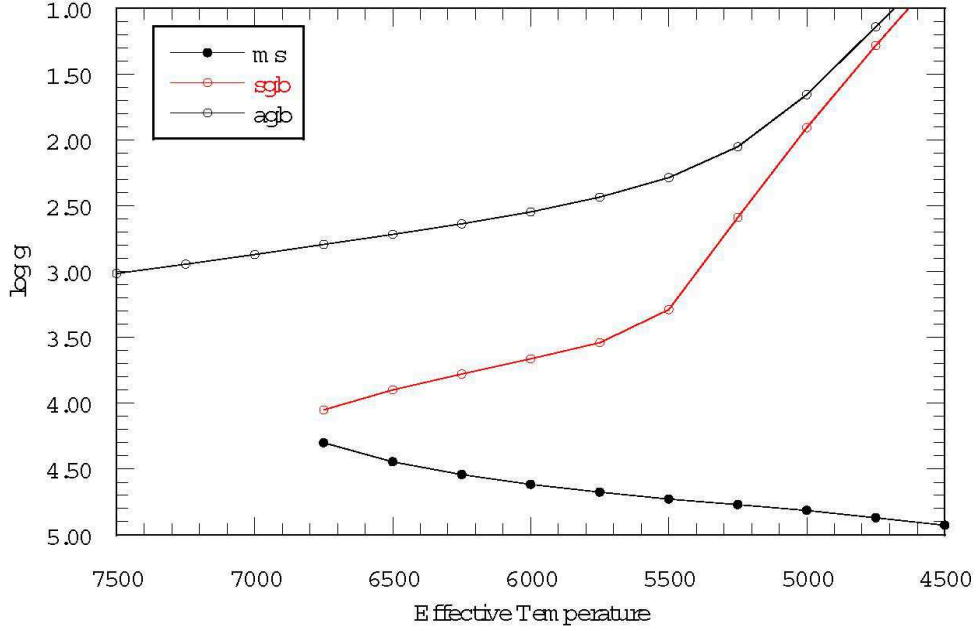


Fig. 1.— Isochrone from Pietrinferni et al. (2006) for 12 Gyrs.

temperatures with older age. As can be seen from the figure, for a given temperature, there are normally only three different possible values for  $\log g$  for a halo star, depending on whether the star is on the main-sequence (MS), on the subgiant/giant branch (SGB) or on the horizontal branch (HB) or asymptotic giant branch (AGB). Cooler than about 5500K it is generally quite easy to choose between a MS ( $\log g = 5$ ), a GB ( $\log g = 3.5$ ) and a HB star ( $\log g = 2.5$ ) but near the MS turnoff the gravity differences are quite small and more difficult to discern.

The Balmer discontinuity is an obvious feature to measure in the spectra of late-type halo stars in order to determine  $\log g$ . Blueward of 3636Å the continuous opacity is mainly H-, whereas redward it is H- plus HI. As  $\log g$  (and  $\log P_e$ ) decreases, the H- opacity decreases and the size of the Balmer discontinuity increases. But as the HI opacity decreases steeply with decreasing temperature, the Balmer jump becomes less sensitive to changes in  $\log g$ .

Although low dispersion spectra are regularly taken of halo stars in order to measure the HK lines of CaII and the H $\delta$  line for metallicity and temperature estimates, little or no effort is put into measuring the Balmer discontinuity. I think that there are three main reasons for this. Firstly, as the Balmer discontinuity is near the confluence of the hydrogen lines the continuum is changing rapidly and it seems impossible to unequivocally extrapolate a curved line that fits the continuum from the 4100Å to 4800Å region where the continuum

is well defined. Secondly, the sensitivity of most spectrographs and CCDs decreases rapidly below 3900Å leading many people to think there is little point in observing below 3600Å. And finally, many think that it may be possible to overcome these difficulties only if a full relative-absolute spectrophotometric calibration is undertaken and this seems like too much effort for uncertain return.

This paper aims to show how, with a minimal amount of extra effort at both the telescope and with the data reduction, the Balmer jump can be readily measured and compared with similar data from the detailed grid of synthetic spectra provided by Munari et al. (2005).

## 2. Techniques

### 2.1. Atmospheric dispersion

When doing ground-based spectroscopy in the UV/blue it is highly desirable that the effect of atmospheric dispersion is minimised either by using an atmospheric dispersion corrector (Filippenko 1982) or by rotating the spectrograph slit so that it is parallel to the atmospheric dispersion. Otherwise, at large zenith distances, if the guider is centering the green or red image, a significant proportion of the UV/blue light will miss the slit. But, as the Balmer jump is measured at one wavelength, it is not absolutely essential to measure the same proportion of light at all wavelengths. However, although a reasonable discontinuity may be measured under these circumstances, any possibility of measuring a temperature sensitive slope or color such as B-V is lost. If an atmospheric dispersion corrector is unavailable, spectra should be taken with the slit tracking the parallactic angle or the star should be acquired in that mode and then observed with the position angle fixed to use an offset guide star in an alt-az telescope.

### 2.2. Division by black-body spectrum

Bessell (1999) discusses the advantages of observing smooth spectrum stars as part of any observing program. After the raw spectra have been extracted, the first step is to divide all spectra by the normalised spectrum of a star with a near-black-body energy distribution.

There are several near-continuous bright white dwarfs well suited for such division. These are EG131 and L745-46a which are accessible in opposite seasons together with vMa2 and two carbon-rich white dwarfs LHS 43 (Bessell 1999) and LHS 4043 (Dufour et al 2005). It is necessary to remove the weak C<sub>2</sub> bands from the carbon WDs and the CaII HK and

MgI lines from L745-46a and vMa2, or fit a line through the continuum before division. Greenstein & Liebert (1990) and Bergeron et al. (2001) discuss the spectra of these stars while Koester & Wolff (2000) and Dufour et al (2005) discuss the theoretical fluxes of some of the stars.

There are two main reasons for dividing by a normalised near-BB spectrum. Firstly, in the red it removes most of the atmospheric (telluric) absorption lines and secondly, for both blue and red spectra it removes most of the instrumental response due to vignetting, grating blaze, filters, mirrors and CCD response. The net effect of this division is to provide spectra in which the continuum level changes slowly and smoothly with wavelength that in turn means the corrections (with wavelength) to place the fluxes on a relative absolute flux scale can be well fitted with a smooth low order polynomial or spline.

### 2.3. Linearisation of the continuum

An unanticipated dividend of the division by a warm near-BB spectrum was the fact that the continuum levels of FGK stars above and below the Balmer jump were transformed from curves into almost straight lines. This enables the continua to be extrapolated with confidence to  $3636\text{\AA}$  and the Balmer jump measured accurately and consistently.

Division by EG131, black-body temperature about 11800K, straightens the continuum in stars with temperatures from 7500K to 5000K. Division by the cooler L745-46a ( $\approx 8600\text{K}$ ) leaves some residual curvature for spectra hotter than 6500K but is good for cooler stars. The two carbon-rich white dwarfs LHS43 and LHS4043 have intermediate black-body temperatures to EG131 and L745-46a; vMa2 is cooler.

Fig. 2 shows examples of raw extracted blue spectra obtained with the Double Beam Spectrograph (DBS) on the ANU 2.3m telescope. The data has not been flat fielded. From the top, are the white dwarf LHS43 and the halo stars G64-12 (sdF0; 6500K/4.0/-3.4), HD 84937 (sdF5; 6200K/4.0/-2.3), G24-3 (sdF8; 5900K/4.2/-1.7), CD -38 245 (4800K/1.5/-4.1). The bracketed quantities are the approximate stellar parameters of the stars. The spectra are offset by 0.2 divisions for clarity.

Fig. 3 shows the same raw spectra divided by the spectrum of EG131. The weak carbon bands in LHS43 and the Balmer jumps in the halo stars are much more obvious and easier to measure in the divided spectra.

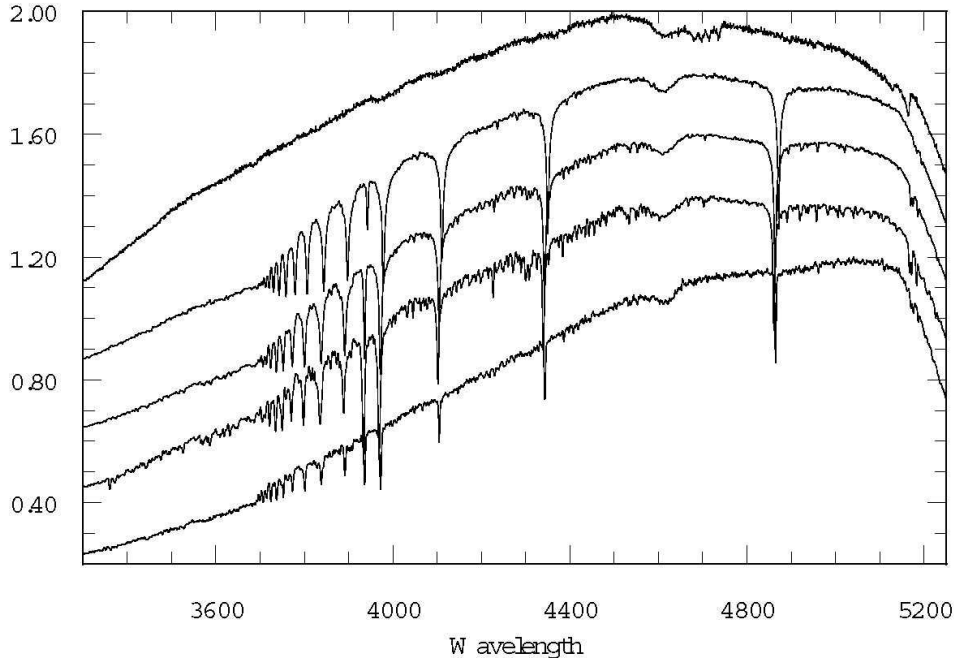


Fig. 2.— Raw extracted blue 2.3m spectra. See text for details

### 3. Theoretical fluxes- model synthetic spectra

Line-blanketed fluxes are available for the ATLAS9 and MARCS grid of model atmospheres. The Munari et al. (2005) ATLAS9 synthetic spectra at  $1\text{\AA}$  resolution are particularly useful. The MARCS sampled photospheric fluxes, available on their website (<http://marcs.astro.uu.se/>) are provided with a warning that they are not likely to give a good representation of the integrated fluxes in a limited wavelength region. But they look adequate for the lowest metallicities.

Fig. 4 shows Munari synthetic flambda spectra for an abundance of  $[\text{Fe}/\text{H}] = -2.5$ , temperature 5750K and three different effective gravities. The spectra have been smoothed to  $3\text{\AA}$  resolution the same as the DBS data. The Balmer discontinuity at  $3636\text{\AA}$  can be seen, but the slope of the continuum redward of this limit makes it difficult to measure it.

The synthetic spectra can also divided by a 11800K blackbody to measure the theoretical Balmer jumps more reliably. Fig. 5 are the same 5750K spectra divided by a 11800K black-body. Fig. 6 to 10 show similarly divided Munari synthetic spectra for several more temperatures and sets of gravities appropriate for main-sequence, giant-branch and horizontal or asymptotic giant branch stars. For each temperature plot, the divided spectra have been normalized at  $5300\text{\AA}$  and are plotted with equal offsets for better visibility. One can

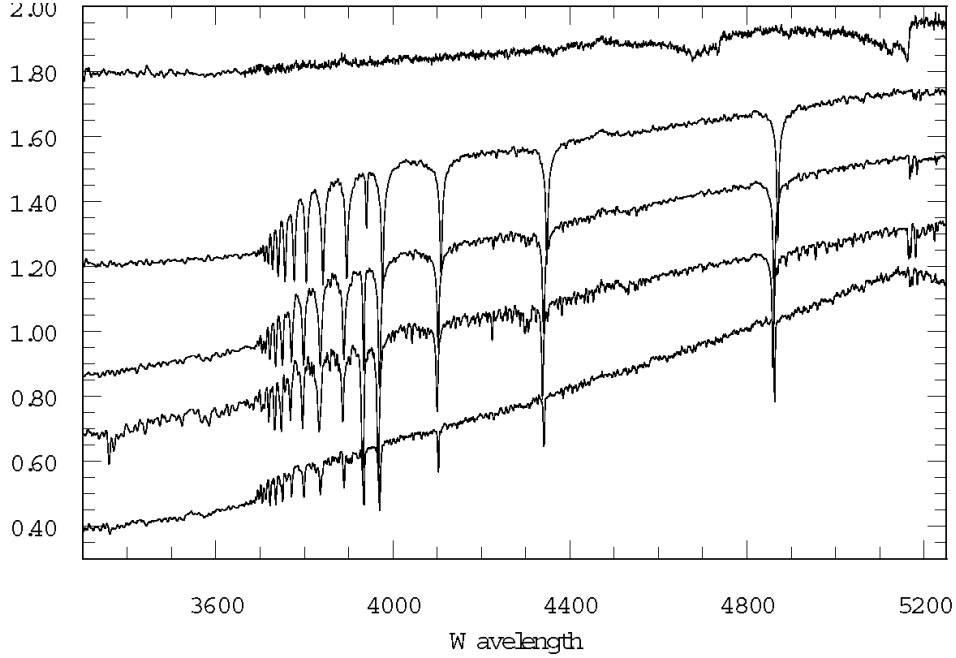


Fig. 3.— Same stars as in Fig.2 but divided by EG131.

draw straight lines through the continua on the various figures to see how linear the continua of the divided observed and synthetic spectra are and how well defined the Balmer jumps are, even when they are small.

## 4. Balmer jump measurements

### 4.1. Theoretical spectra

The model spectra were wavelength crunched and then smoothed to approximate the observed medium resolution spectra. The Munari spectra were smoothed to  $5\text{\AA}$  resolution, the MARCS fluxes to  $6\text{\AA}$  resolution. All model spectra were divided by a 11800 black-body, plotted up and the Balmer jumps measured by hand as for the observed spectra. The size of the Balmer jump in magnitudes are given in Table 1 and Table 2. The depth of the  $H\delta$  line was also measured as it is a good temperature indicator, but for comparison with observations it is necessary to carefully match the resolution whereas the Balmer jump measurement is not as sensitive to the resolution. The theoretical b-y, B-V, V-R and V-I colors were also computed for the synthetic spectra.

In Fig. 11 are plotted the measured Balmer jumps for the Munari spectra ( $[\text{Fe}/\text{H}]=-2.5$ , cross;

Table 1. MUNARI et al spectra

Te	log g	[Fe/H]=-1			[Fe/H]=-1.5			[Fe/H]=-2.5		
		BJ	b-y	V-I	BJ	b-y	V-I	BJ	b-y	V-I
6500	4.5	0.40	0.289	0.545	0.36	0.293	0.551	0.31	0.300	0.556
6500	4.0	0.52	0.279	0.532	0.48	0.283	0.538	0.44	0.290	0.543
6500	3.5	0.67	0.269	0.519	0.63	0.272	0.523	0.59	0.278	0.528
6250	4.5	0.30	0.319	0.600	0.28	0.323	0.605	0.23	0.330	0.611
6250	4.0	0.41	0.311	0.591	0.39	0.314	0.597	0.34	0.321	0.602
6250	3.5	0.52	0.303	0.580	0.51	0.306	0.585	0.46	0.311	0.590
6000	4.5	0.23	0.349	0.656	0.18	0.354	0.662	0.17	0.362	0.668
6000	4.0	0.31	0.344	0.650	0.28	0.347	0.656	0.24	0.354	0.661
6000	3.5	0.42	0.338	0.643	0.39	0.340	0.647	0.33	0.346	0.652
5750	4.5	0.16	0.381	0.716	0.13	0.387	0.722	0.09	0.397	0.729
5750	4.0	0.23	0.377	0.712	0.20	0.381	0.717	0.14	0.389	0.722
5750	3.5	0.31	0.373	0.706	0.28	0.375	0.711	0.22	0.382	0.716
5500	4.5	0.11	0.413	0.778	0.09	0.422	0.786	0.03	0.437	0.796
5500	4.0	0.16	0.412	0.776	0.13	0.417	0.781	0.07	0.427	0.788
5500	3.5	0.23	0.410	0.772	0.18	0.414	0.778	0.12	0.420	0.783
5250	4.5	0.07	0.447	0.848	0.07	0.459	0.856	0.00	0.482	0.872
5250	3.0	0.20	0.450	0.842	0.16	0.453	0.848	0.11	0.458	0.853

Table 2. MARCS statistical line opacity spectra

Te	log g	[Fe/H]=-1			[Fe/H]=-1.5			[Fe/H]=-2.5		
		BJ	b-y	V-I	BJ	b-y	V-I	BJ	b-y	V-I
6500	4.5	0.40	0.285	0.540	0.39	0.290	0.546	0.33	0.297	0.553
6500	4.0	0.55	0.277	0.528	0.50	0.281	0.535	0.47	0.287	0.541
6500	3.5	0.67	0.267	0.515	0.64	0.270	0.520	0.61	0.277	0.525
6250	4.5	0.33	0.313	0.595	0.30	0.318	0.601	0.26	0.326	0.607
6250	4.0	0.43	0.307	0.587	0.40	0.312	0.593	0.34	0.318	0.599
6250	3.5	0.54	0.300	0.576	0.51	0.303	0.582	0.47	0.309	0.587
6000	4.5	0.30	0.342	0.651	0.22	0.349	0.657	0.16	0.357	0.664
6000	4.0	0.36	0.339	0.646	0.30	0.343	0.652	0.24	0.350	0.657
6000	3.5	0.42	0.334	0.639	0.39	0.337	0.644	0.34	0.344	0.649
5750	4.5	0.24	0.371	0.711	0.19	0.379	0.716	0.10	0.392	0.724
5750	4.0	0.28	0.371	0.706	0.23	0.376	0.712	0.15	0.385	0.718
5750	3.5	0.34	0.368	0.703	0.30	0.372	0.708	0.24	0.378	0.713
5500	4.5	0.24	0.403	0.776	0.15	0.412	0.780	0.06	0.429	0.789
5500	4.0	0.27	0.403	0.772	0.15	0.409	0.777	0.09	0.422	0.784
5500	3.5	0.30	0.403	0.770	0.20	0.408	0.774	0.13	0.416	0.780
5250	4.5	0.22	0.437	0.850	0.11	0.445	0.852	0.00	0.472	0.864
5250	3.5	0.22	0.441	0.842	0.09	0.444	0.845	0.06	0.458	0.853



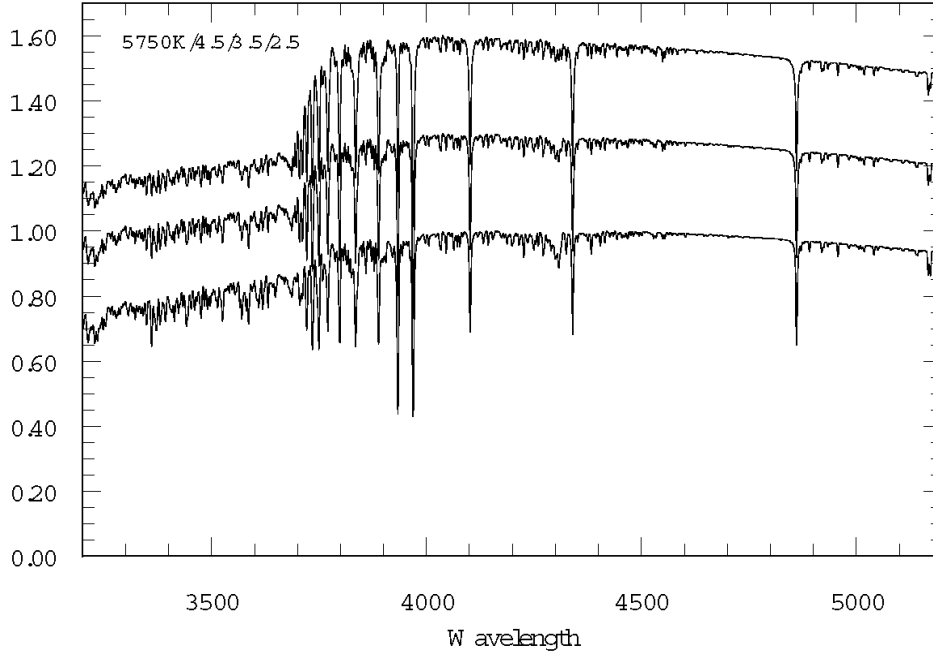


Fig. 4.— Synthetic flambda spectra for  $[\text{Fe}/\text{H}]=-2.5$ , 5750K and  $\log g=4.5, 3.5, 2.5$

$[\text{Fe}/\text{H}]=-1.5$  crossed open square) and the MARCS spectra ( $[\text{Fe}/\text{H}]=-2.5$ , filled circle;  $[\text{Fe}/\text{H}]=-1.5$  open circle). There is good general agreement for the two grids, except for the coolest and strongest line spectra where as noted above, the MARCS sampled photospheric fluxes are not likely to give a good representation of the integrated flux in a limited wavelength region. Full spectrum synthesis is needed for the MARCS models to properly compare them. However, both sets of theoretical spectra show that for temperatures above 5500K the Balmer jump can readily distinguish main sequence and subgiant branch stars, while for temperatures at around 5000K and 5250K, only gravities below  $\log g=3.0$  can be distinguished from  $\log g=4.5$  main sequence stars. Cooler than 5000K the Balmer jump is virtually impossible to measure except in the most extreme metal-poor stars.

The model spectra show that the measured Balmer jump increases as the metallicity increases due probably to the greater strength of metal-line blanketing in the UV than in the blue.

## 4.2. Observations

There are several excellent spectral libraries that can be used for Balmer jump measurements and comparison with the models. The best library is probably the Next Generation Spectral Library of STIS data by Gregg (2005) (<http://lifshitz.ucdavis.edu/~mgregg/gregg/ngsl/download.html>). Pre-

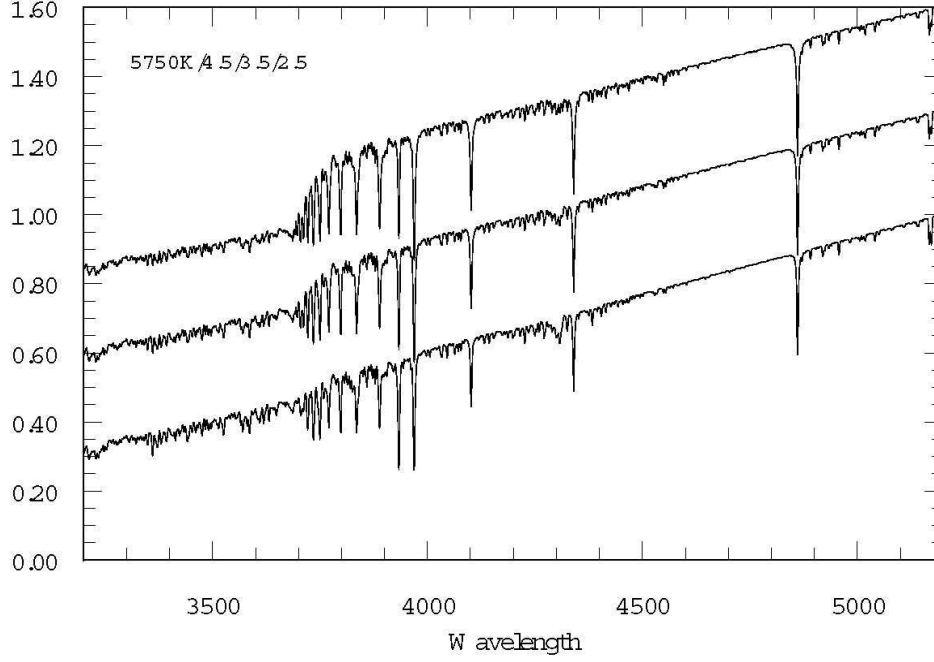


Fig. 5.— 11800K BB divided spectra for  $[\text{Fe}/\text{H}]=-2.5$ , 5750K and  $\log g=4.5, 3.5, 2$

liminary versions of the spectra have been kindly provided by Michael Gregg and Jesus Maiz Ap-  
pelaniz. The Sanchez-Blanco et al. (2006) library (<http://www.ucm.es/info/Astrof/miles/miles.html>)  
is of similar quality and resolution but has shorter wavelength coverage (3500Å - 7500Å. .

Table 3 lists the measured Balmer jumps of the STIS spectra together with the Hipparcos  $M_v$   
and colors computed from the spectra.

Table 3. balmer jumps measured from STIS spectra

Star	[Fe/H]	Mv	BJ	b-y	V-I	V-R
bd092860		4.31	0.39	0.413	0.798	0.393
bd174708	-1.7	4.09	0.39	0.316	0.629	0.306
bd292091	-2.1	5.38	0.16	0.372	0.731	0.352
bd371458	-1.6	2.73	0.20	0.409	0.774	0.373
bd413931	-1.8	6.05	0.08	0.415	0.809	0.401
bd423607	-2.0	5.51	0.19	0.344	0.639	0.308
bd511696	-1.4	5.58	0.19	0.394	0.778	0.380
bd592723	-1.7	5.22	0.33	0.337	0.708	0.340
bd720094	-1.6	3.99	0.40	0.303	0.671	0.315
bd-122669	-1.5	4.04	0.65	0.227	0.500	0.236
cd-3018140	-2.2	4.26	0.42	0.298	0.570	0.270
g115-58	-1.4	3.62	0.37	0.325	0.696	0.335
g029-023	-2.0	2.78	0.39	0.338	0.684	0.334
g88-27	-1.9	-0.82	0.36	0.316	0.654	0.312
hd002665	-2.0	4.34	0.11	0.537	1.005	0.494
hd002857	-1.6	1.24	1.38	0.085	0.216	0.089
hd006755	-1.6	2.16	0.15	0.489	0.957	0.467
hd016031	-1.8	4.46	0.37	0.305	0.629	0.298
hd019445	-2.0	5.10	0.27	0.329	0.681	0.319
hd044007	-1.7	1.62	0.09	0.548	1.045	0.511
hd045282	-1.5	2.33	0.17	0.448	0.861	0.422
hd063791	-1.7	-0.89	0.00	0.588	1.127	0.549
hd087140	-1.6	2.18	0.21	0.461	0.946	0.452
hd094028	-1.3	4.63	0.30	0.327	0.685	0.324
hd111721	-1.1	0.56	0.13	0.507	0.981	0.480
hd128279	-2.1	1.90	0.18	0.449	0.908	0.432
hd132475	-1.3	3.73	0.28	0.363	0.778	0.365
hd134439	-1.5	6.74	0.04	0.424	0.857	0.429
hd134440	-1.5	7.08	0.02	0.516	1.059	0.538
hd163346		0.30	0.99	0.380	0.839	0.403
hd163810	-1.4	5.00	0.20	0.384	0.745	0.368
hd165195	-2.2	4.02		0.894	1.533	0.774
hd184266	-1.8	0.17	0.55	0.418	0.817	0.400

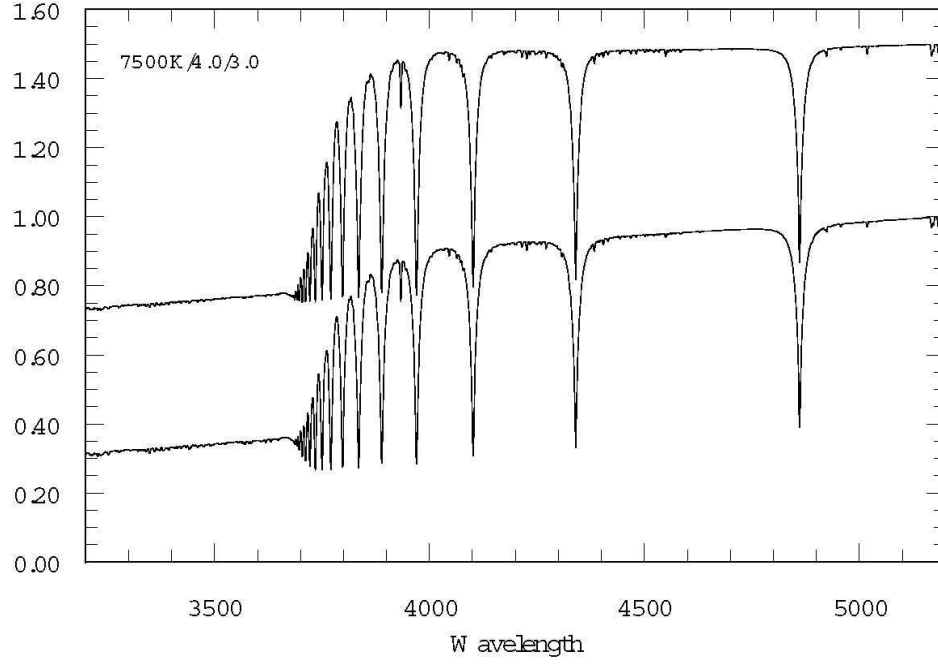


Fig. 6.— 11800K BB divided spectra for  $[\text{Fe}/\text{H}]=-2.5$ , 7500K and  $\log g=4.0, 3.0$ .

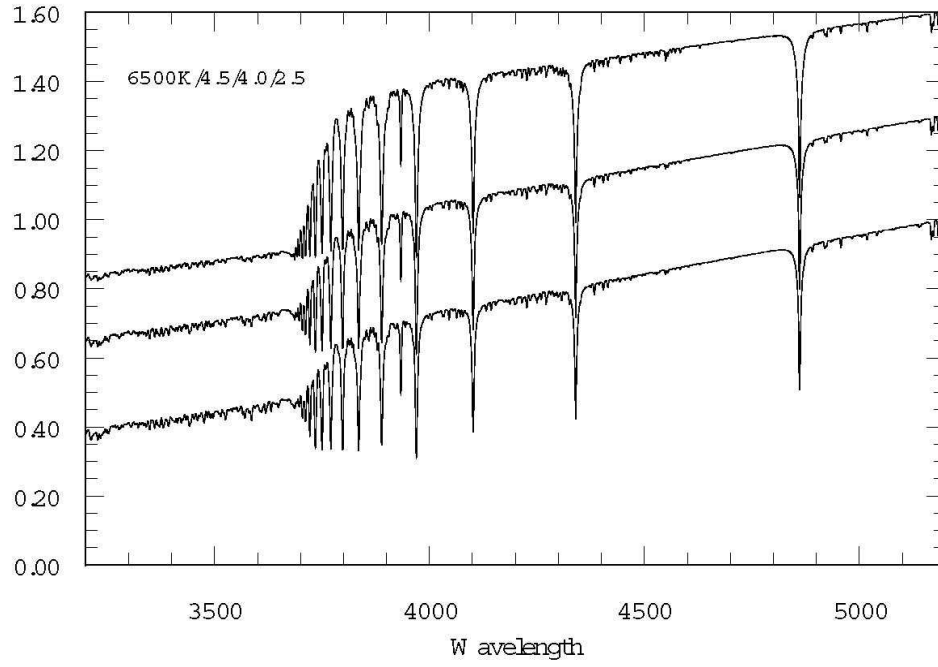


Fig. 7.— 11800K BB divided spectra for  $[\text{Fe}/\text{H}]=-2.5$ , 6500K and  $\log g=4.5, 4.0, 2.5$ .

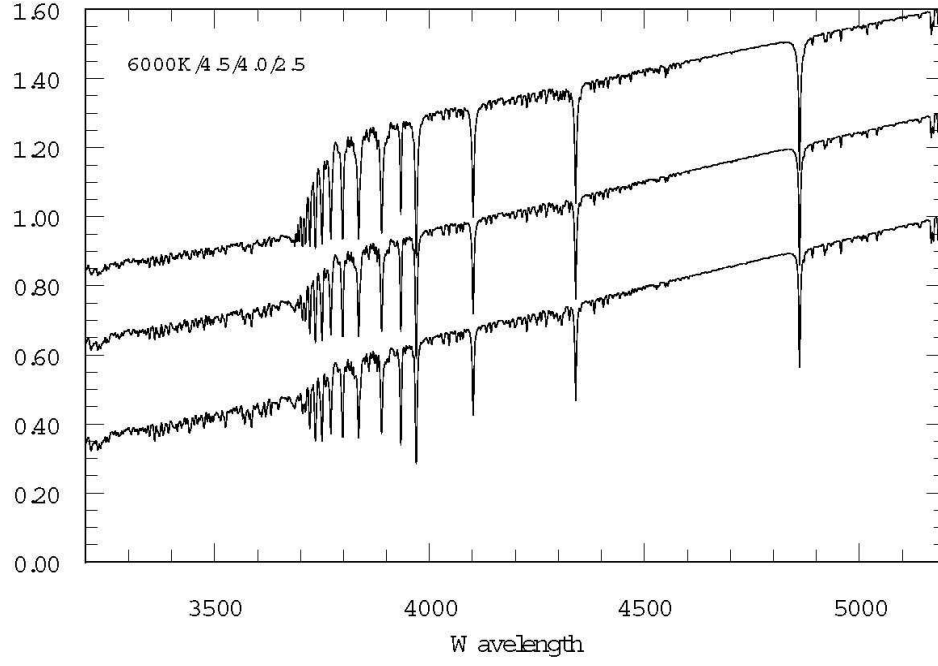


Fig. 8.— 11800K BB divided spectra for  $[\text{Fe}/\text{H}]=-2.5$ , 6000K and  $\log g=4.5, 4.0, 2.5$ .

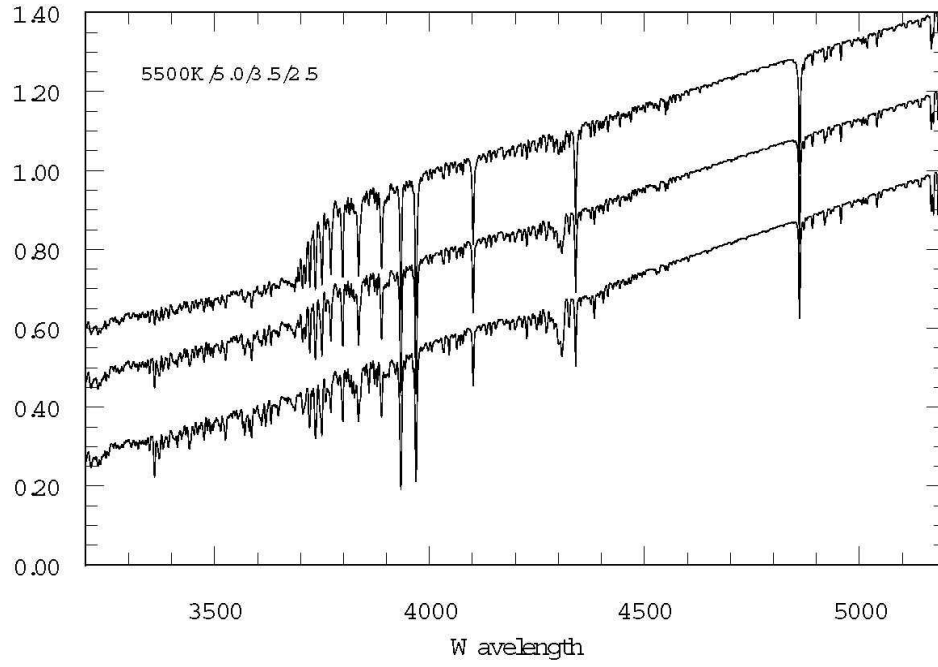


Fig. 9.— 11800K BB divided spectra for  $[\text{Fe}/\text{H}]=-2.5$ , 5500K and  $\log g=5.0, 3.5, 2.0$ .

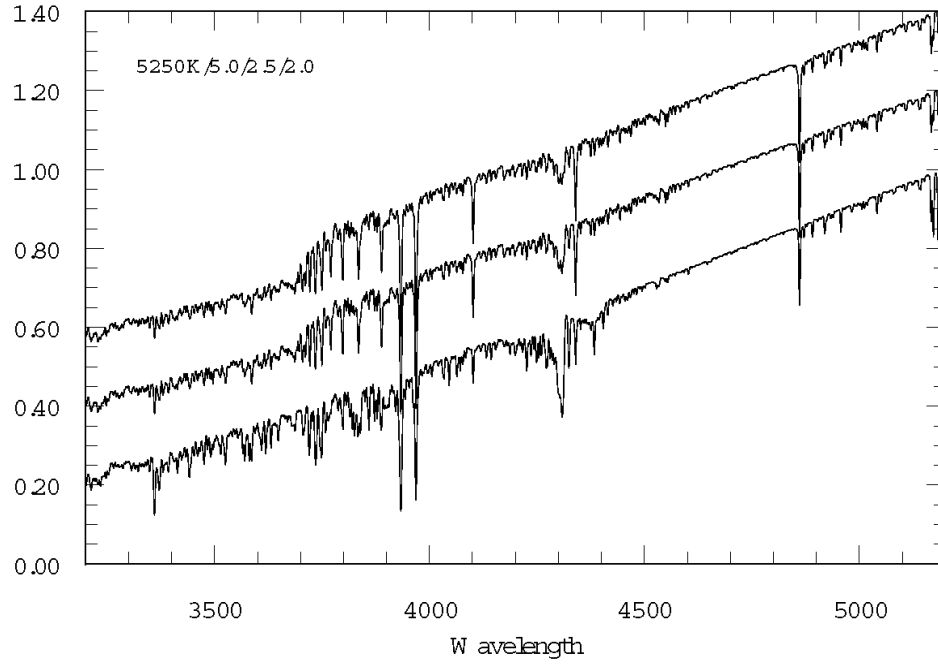


Fig. 10.— 11800K BB divided spectra for  $[\text{Fe}/\text{H}]=-2.5$ , 5250K and  $\log g=5.0, 2.5, 2.0$ .

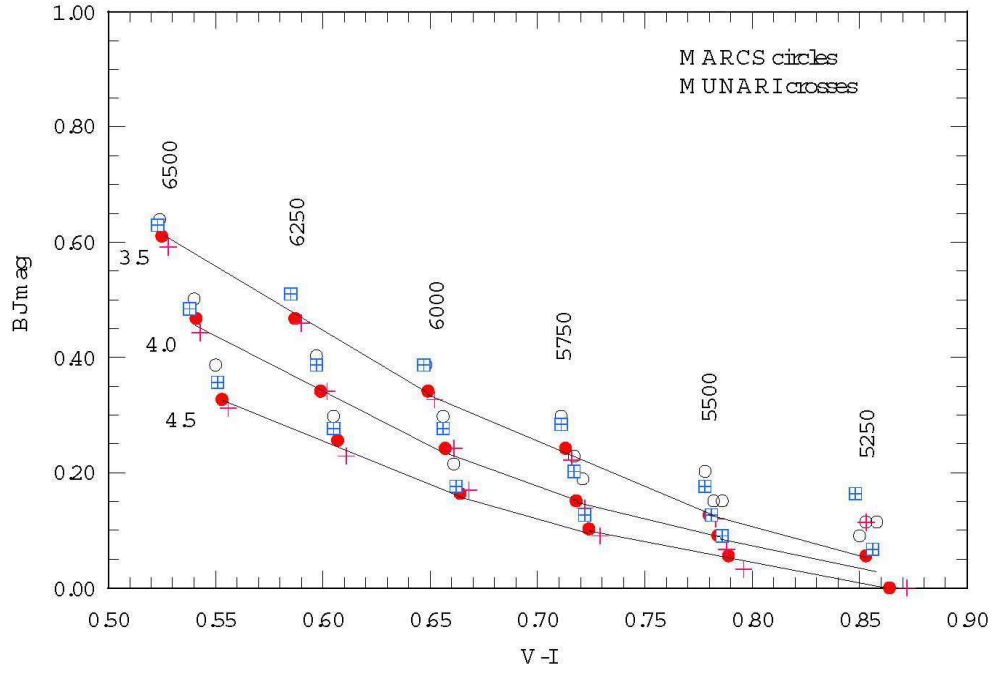


Fig. 11.— Measured Balmer jumps versus  $V-I$  color for model spectra for  $[Fe/H]=-1.5$  and  $-2.5$ . Connecting lines are drawn through points for the same gravity for the  $[Fe/H]=-2.5$  spectra.

Table 4 lists the measured Balmer jumps of the MILES spectra together with the atmospheric parameters from Cenarro et al. (2007) and the b-y and B-V colors computed from the spectra.

In Fig. 12, the  $M_v$  versus b-y diagram for the STIS spectra is shown together with a halo isochrone. Some of the  $M_v$  values are poorly determined because of large uncertainties in the parallax and there are at least 4 stars whose absolute magnitudes are in disagreement with their Balmer jump measurements shown in Fig.13.

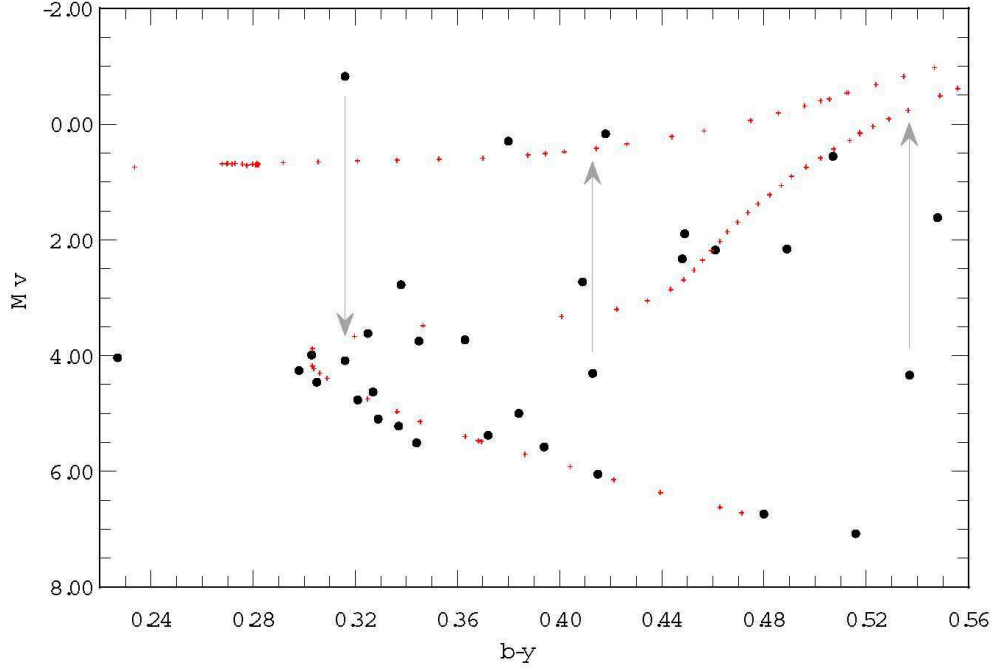


Fig. 12.— The  $M_v$  versus b-y diagram for the selection of STIS spectra of low metallicity stars listed in Table 3. A halo isochrone is shown for orientation. The lines with arrow heads indicate the appropriate shifts for those stars whose  $M_v$  values are inconsistent with their measured Balmer jumps.

In Fig 13 are plotted the observed Balmer jumps for the STIS sample versus b-y. Lines have

Table 3—Continued

Star	[Fe/H]	$M_v$	BJ	b-y	V-I	V-R
hd284248	-1.4	4.77	0.36	0.321	0.659	0.316
hd345957	-1.3	3.75	0.33	0.345	0.742	0.347



Table 4. Balmer jumps measured from MILES spectra

Star	[Fe/H]	Te	log g	BJ	b-y	B-V
hd002665	-2.0	5013	2.35	0.22	0.509	0.720
hd002796	-2.3	4950	1.36	0.28	0.520	0.724
hd019445	-2.1	5920	4.40	0.26	0.345	0.445
hd045282	-1.4	5350	3.20	0.22	0.458	0.658
hd046703	-1.6	6000	0.40	1.20	0.302	0.421
hd064090	-1.8	5450	4.45	0.08	0.424	0.608
hd074000	-2.0	6170	4.20	0.37	0.322	0.407
hd084937	-2.2	6230	4.00	0.45	0.301	0.374
hd085773	-2.2	4460	1.00	0.00	0.737	1.046
hd088609	-2.6	4513	1.30		0.676	0.941
hd094028	-1.5	5950	4.20	0.31	0.347	0.462
hd103095	-1.4	5030	4.60	0.09	0.487	0.754
hd122563	-2.6	4570	1.12	0.09	0.653	0.903
hd140283	-2.5	5690	3.60	0.30	0.361	0.474
hd165195	-2.2	4470	1.10		0.830	1.219
hd187111	-1.8	4260	0.60		0.809	1.215
hd188510	-1.6	5490	4.70	0.23	0.403	0.591
hd218502	-1.8	6030	3.80	0.43	0.309	0.414
hd218857	-1.9	5080	2.40	0.18	0.492	0.705
hd219617	-1.4	5880	4.00	0.26	0.348	0.478
hd221170	-2.1	4470	1.00		0.712	1.049
hd237846	-2.6	4960	1.80	0.20	0.489	0.668
hd251611	-1.7	5350	3.80	0.15	0.474	0.664
hd284248	-1.6	6025	4.20	0.39	0.328	0.422

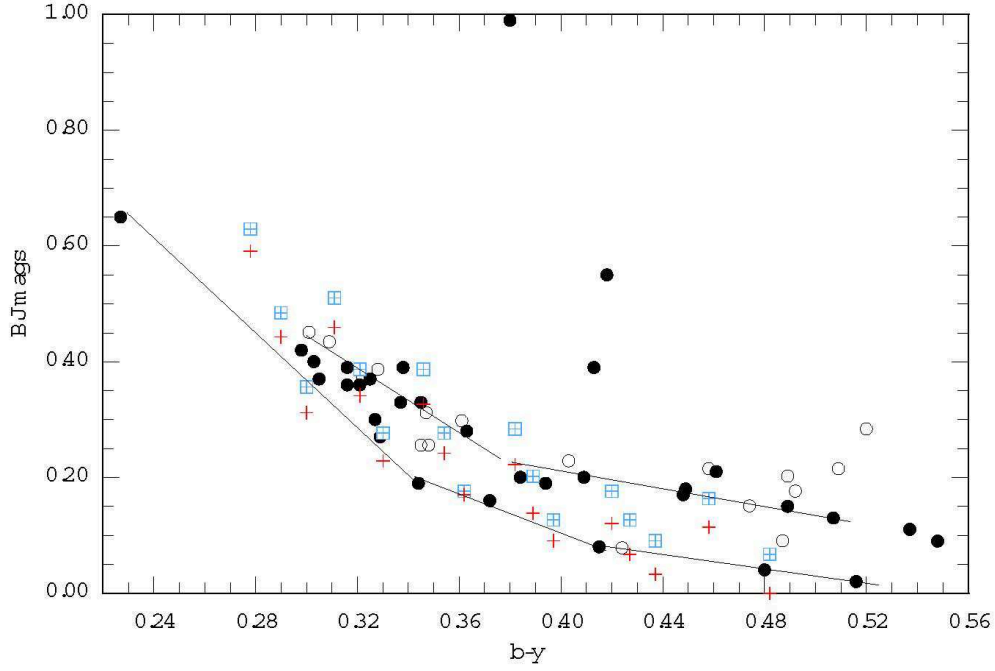


Fig. 13.— Measured Balmer jumps versus  $b-y$  color for the STIS stars (closed circles) and MILES spectra (open circles). Lines have been drawn to connect the stars on the main-sequence, the subgiant and the giant branch as identified in Fig 12. The same relation for the Munari spectra for  $[\text{Fe}/\text{H}]=-1.5$  plotted in Fig. 11 is also shown.

been drawn through the main-sequence stars, the subgiant and giant branch stars as indicated from Fig 12. The stars whose  $M_v$  values differ significantly from their Balmer jumps are marked in Fig 12. The theoretical values for the Munari  $[\text{Fe}/\text{H}]=-1.5$  and  $-2.5$  spectra are also shown for  $\log g = 3.5, 4.0$  and  $4.5$  and temperatures  $T_e=6500\text{K}, 6250\text{K}, 6000\text{K}, 5750\text{K}, 5500\text{K}$  and  $5250\text{K}$ . The Balmer jumps from the synthetic spectra are in good agreement with the observed loci of metal-poor stars. Precise derivation of the gravities of individual stars involves knowledge of the metallicity and temperature (and the reddening if fluxes are used), which is beyond the scope of this paper.

## 5. Summary

Dividing extracted raw spectra by the spectrum of a warm near-blackbody object such as EG131, L745-46a, LHS43 or LHS4043 results in spectra whose continua above and below the Balmer discontinuity are close to straight lines thus making it easy to measure the size of the Balmer jump accurately.

The recommendation is to observe a warm near-black-body star at least once a run for each grating setting used then divide all extracted raw spectra by a template made from the normalised extracted blackbody spectrum by removing any obvious lines or bands it may have or fitting the continuum. In order to accurately measure the theoretical Balmer jumps from synthetic spectra such as those of Munari et al. (2005), it is also important to divide the synthetic spectra by the normalised theoretical blackbody spectrum of similar black-body temperature to the template star used.

Having followed these recommendations and measured the Balmer jump, the effective gravity can be derived from the model spectra. If the effective temperature of the FGK star is known to within 100K the Balmer jump will yield an effective gravity to about 0.2 dex for the hotter stars and 0.5 dex for the cooler stars, sufficient precision to determine whether the star is a main-sequence, giant branch or horizontal/asymptotic giant branch star.

Best spectrophotometric results are achieved if an atmospheric dispersion corrector is used or if the spectrograph is rotated to put the parallactic angle along the slit. This is not essential to measure the monochromatic Balmer jump but it does ensure that the spectra can be accurately calibrated onto a relative absolute flux scale and that other temperature sensitive colors can be derived.

## 6. Acknowledgments

I am grateful to Dr Lajos Balazs, Director of Konkoly Observatory and Dr Katalin Olah for their hospitality during the writing of this paper. I am also grateful to Dr Fiorella Castelli for providing the synthetic spectra; to Dr Santi Cassisi for computing additional isochrones and to Dr Michael Gregg and Dr Jesus Maiz Appellaniz for the preliminary NGSL STIS spectra.

*Facilities:* SSO: 2.3m (DBS) HST: STIS

## REFERENCES

- Bergeron, P., Leggett, S.K., Ruiz, M.T. 2001, ApJ, 133, 413
- Bessell, M.S. 1999, PASP, 111, 1426
- Cenarro, A.J., Peletier, R.F., Sanchez-Blazquez, P., Selam, S.O., Toloba, E., Cardiel, N., Falcon-Barroso, J., Gorgas, J., Jimenez-Vicente, J., Vazdekis, A. 2007, MNRAS, 374, 664
- Dufour, P., Bergeron, P., Fontaine, G. 2005, ApJ, 627, 404
- Filippenko, A.V. 1982, PASP, 94, 715

- Gregg, M.D., Silva, D., Rayner, J., Worthy, G., Valdes, F., Pickles, A., Rose, J., Carney, B., Vacca, W. 2005 in The 2005 HST Calibration Workshop (Eds. A.M. Koekemoer, P. Goudfrooij and L.L. Dressel:Space Telescope Science Institute, 2005), p209
- Greenstein, J.L., Liebert, J.W. 1990, ApJ, 360, 662
- Koester, D., Wolff, B. A&A, 357, 587
- Munari, U., Sordo, R., Castelli, F., Zwitter, T. 2005, A&A, 442, 1127
- Pietrinferni, A., Cassisi, S., Salaris, M., Castelli, F. 2006, ApJ, 642, 797
- Salasnich, B., Girardi, L., Weiss, A., Chiosi, C. 2000, A&A, 361, 1023
- Sanchez-Blazquez,P., Peletier, R.F.,Jimenez-Vicente,J., Cardiel,N., Cenarro,A.J., Falcon-Barroso,J., Gorgas,J., Selam,S., Vazdekis,A.2006, MNRAS, 371, 708
- VandenBerg, D.A. 2000, ApJS, 129, 315